Applied Catalysis B: Environmental 180 (2016) 283–290

Contents lists available at ScienceDirect

Applied Catalysis B: Environmental

journal homepage: www.elsevier.com/locate/apcatb

Surface Ba species effective for photoassisted NO_x storage over Ba-modified TiO_2 photocatalysts

Akira Yamamoto[a,b], Yuto Mizuno[a], Kentaro Teramura[a,b,c,*], Saburo Hosokawa[a,b], Tsunehiro Tanaka[a,b,*]

[a] Department of Molecular Engineering, Graduate School of Engineering, Kyoto University, Kyotodaigaku Katsura, Nishikyo-ku, Kyoto 615-8510, Japan
[b] Elements Strategy Initiative for Catalysts & Batteries (ESICB), Kyoto University, Kyotodaigaku Katsura, Nishikyo-ku, Kyoto 615-8520, Japan
[c] Precursory Research for Embryonic Science and Technology (PRESTO), Japan Science and Technology Agency (JST), 4-1-8Honcho, Kawaguchi, Saitama 332-0012, Japan

ARTICLE INFO

Article history:
Received 19 May 2015
Received in revised form 15 June 2015
Accepted 17 June 2015
Available online 23 June 2015

Keywords:
Photocatalyst
Nitrogen oxides
NO_x
Titanium dioxide
NO_x storage

ABSTRACT

Surface modification of a TiO_2 photocatalyst with Ba species was investigated in photoassisted nitrogen oxide (NO_x) storage under UV-light irradiation. The NO_x storage capacity in the Ba-modified TiO_2 photocatalyst was 1.4 times higher than that of the non-modified TiO_2 photocatalyst. Structure and role of the surface Ba species on a TiO_2 surface were characterized using temperature programmed reaction (TPR), diffuse reflectance infrared Fourier transform (DRIFT) spectroscopy, X-ray diffraction (XRD), X-ray photoemission spectroscopy (XPS), and transmission electron microscopy (TEM). The characterization results suggested that Ba–Ti mixed oxides with a two-dimensional layer and amorphous structure on a TiO_2 surface were generated via decomposition of $Ba(NO_3)_2$ precursors by O_2 pretreatment at 773 K. Based on the results of the characterizations and the reactions, the generated Ba–Ti mixed oxides on a TiO_2 surface stored NO_x more densely than the TiO_2 surface; therefore, the generation improved the activity in the photoassisted NO_x storage under UV-light irradiation.

1. Introduction

Control of nitrogen oxide (NO_x) emission in exhaust gas from engines is strongly required in terms of air purification. Many researchers and engineers have been challenged to develop efficient de-NO_x technologies [1]. At the stoichiometric air-to-fuel (A/F) ratio of 14.7, three way catalysts are used for the NO_x removal [2,3]. However, under lean conditions (air-rich, A/F ratio: 20–65), typical three way catalysts cannot efficiently decompose the NO_x to harmless N_2 although the lean operation of the engines leads to fuel economy and decreases of CO_2 emission [4,5]. Two technologies have been developed for the removal of NO_x under the lean condition: selective catalytic reduction (SCR) and NO_x storage and reduction (NSR). In the SCR, NH_3, which is produced by decomposition of urea is introduced into the exhaust gas, and the introduced NH_3 reduces the NO_x to N_2. The SCR have been investigated by many researchers since 1970s. V_2O_5-based catalysts [6–8] and Fe- or Cu-zeolite catalysts [9] show high activity over 473 K. This technology is widely used in stationary emission sources and mobile emission sources including diesel engines in vehicles and trucks. However, the NO_x removal efficiency is low below 473 K.

Low-temperature removal of NO_x is highly desired in exhaust gas from vehicle engines. Regulation of NO_x emission has become severe year by year [10], and a recent report by the International Council for Clean Transportation (ICCT) pointed out the impact of the NO_x emission in the initial stage of engine start-up on the total emission amounts; in the cold start condition below 473 K (approximately 800 s), urea cannot be injected because of the low activity of the catalyst to avoid ammonia slip [11]. Thus, development of low temperature technology for NO_x removal is urgent task to improve the total removal efficiency of NO_x in the cold start condition.

On the other hand, the NSR technology was firstly reported by Toyota researchers in 1995 [5,12]. The NSR catalyst is composed of three components: precious metals, alkali or alkali earth oxides, and supports (e.g., $Pt/BaO/Al_2O_3$) [4]. In the lean condition, NO is oxidized on Pt sites and stored as nitrite (NO_2) or nitrate (NO_3^-) species. At that time, BaO functions as a NO_x storage material. After the NO_x storage in the lean condition, the engine is switched to the fuel-rich condition for a short time by injecting the fuels, and the

* Corresponding authors at: Department of Molecular Engineering, Graduate School of Engineering, Kyoto University, Kyotodaigaku Katsura, Nishikyo-ku, Kyoto 615-8510, Japan. Fax: +81 75 383 2561.
E-mail addresses: teramura@moleng.kyoto-u.ac.jp (K. Teramura), tanakat@moleng.kyoto-u.ac.jp (T. Tanaka).

http://dx.doi.org/10.1016/j.apcatb.2015.06.036
0926-3373/

stored NO_x^- is reduced by the injected fuels into N_2 over Pt sites [4]. The lean and rich cycle operation provides the high NO_x removal efficiency [13]. However, the NSR catalysts also cannot reduce the NO_x efficiently at low temperatures below 473 K [14].

Photocatalysts are promising materials in terms of such a low temperature operation. Until now, several photocatalysts have been reported in the NO oxidation: TiO_2 [15], N-doped TiO_2 [16], metal-modified TiO_2 [17,18], TiO_2–Al_2O_3 binary oxide [19,20]. The reaction mechanism of NO oxidation was also investigated over the TiO_2 photocatalysts [21–28]. Recently, we demonstrated the Ba-modified TiO_2 photocatalysts showed high activity at a practical condition (gas hourly space velocity: 50,000 h^{-1}, NO concentration: 200 ppm) under UV-light irradiation, and Ba modification of TiO_2 greatly enhanced the activity of NO_x storage at low temperature [29]. The activity was improved after the pretreatment in O_2/He gas over 673 K, and the temperature corresponded to the decomposition temperature of $Ba(NO_3)_2$ used as a Ba precursor. Thus, the activated Ba oxide species were generated during the pretreatment. The structure and the role of Ba oxide species are still unclear as the case now stands.

In Pt/BaO/Al_2O_3 system of a typical NSR catalyst, classically, BaO and $BaCO_3$ species were assumed to be NO_x storage materials [4,13]. On the other hand, BaO and Al_2O_3 react at high temperature (>1073 K) to form an aluminate phase, $BaAl_2O_4$ [30–32]. It was previously reported that the $BaAl_2O_4$ was a better NO_x storage material than BaO and/or $BaCO_3$ [30,31], although other groups reported that the generation of $BaAl_2O_4$ decreased the performance [33]. In addition, TiO_2 was added to the NSR catalyst to improve the dispersion of Ba species using a strong interaction between Ba and Ti atoms [34], and the tolerance to sulfur poisoning [35–37], where the high temperature operations resulted in the generation of mix-oxide phase of Ti and Ba [34,38]. (e.g., $BaTiO_3$) In our photocatalytic system, $BaTiO_3$ phase was observed after the pretreatment in O_2/He at 873 K, and the generation caused the decrease of NO_x storage activity [29]. Thus, the generation of mixed oxide phase and the effect on the activity should be considered to explain the role of Ba oxide species. In the present paper, the structure and role of Ba oxide species were investigated in the photoassisted NO_x storage at low temperature to elucidate the Ba oxide species active for the NO_x storage.

2. Experimental

2.1. Materials

TiO_2 (ST-01, Ishihara Sangyo Kaisha, Ltd.) powder was used as purchased. Barium nitrate ($Ba(NO_3)_2$, 99.9%) and barium titanate ($BaTiO_3$) were purchased from Wako Co., Ltd. (Japan). 100–1000 μmol g^{-1} Ba/TiO_2 catalysts were prepared by impregnation using a $Ba(NO_3)_2$ precursor and a water (20 mL) as a solvent.

2.2. Activity tests

Photoassisted NO_x storage was carried out using a fixed bed flow system. The detail was shown elsewhere [29]. Briefly, 0.13 g catalyst granules (diameter: 300–600 μm) were added to a quarts reactor (12 mm × 10 mm × 1 mm, volume: 0.12 mL), and then pretreated at 773 K in 10% O_2/He gas at 50 mL min^{-1} for 1 h. The reaction gas (NO: 200 ppm, O_2: 3%, He: balance) was flowed at 100 mL min^{-1}. A 300 W Xe lamp (PerkinElmer PE300BF) was used as a light source. The NO_x ($NO + NO_2$) in the outlet gas was analyzed using a portable gas analyzer (HORIBA PG-335). Dead time for NO_x breakthrough, which was defined as a time when the outlet concentration of NO_x reached to 2 ppm (conversion of NO: 99%), was used for NO_x breakthrough in the present research.

2.3. Characterization

N_2 adsorption measurement was performed on a Belsorp-miniII (BEL, Japan) at 77 K. The specific surface area (S_{BET}) was estimated from the N_2 adsorption isotherm using Brunauer–Emmett–Teller (BET) method. X-ray diffraction (XRD) measurement was carried out using a Rigaku Ultima IV X-ray diffractometer with Cu-Kα radiation (λ = 1.5406 Å). The crystallite size was determined by the Scherrer equation using the full width at half maximum (FWHM) of the diffraction peak of anatase TiO_2 (1 0 1) plane. Temperature-programmed desorption (TPD) experiment was performed on the same experimental set-up as the activity test in 10% O_2/He gas at 50 mL min^{-1}. After the temperature was kept at 373 K for 30 min, the TPD measurement was started at a heating rate of 5 K min^{-1} up to 973 K. The increase of temperature was also monitored using a thermocouple and an integrator. In situ diffuse reflectance infrared Fourier transform (DRIFT) spectra were measured using an ISDR-600 FTIR spectrometer (JASCO, Japan) equipped with a mercury–cadmium–tellurium (MCT) detector cooled by liquid nitrogen at a resolution of 4 cm^{-1} with 16 co-added scans. The sample powder (50 mg) was placed in a diffuse reflectance cell, which was fitted by a potassium bromide (KBr) window at the top. The gas compositions of the pretreatment and the DRIFT experiment were the same as the activity tests. The catalyst was pretreated at 773 K, and then cooled to 373 K. A 200 W Hg–Xe lamp equipped with a collective lens (San-Ei Electric Co., Ltd., UVF-204S type C) was used as a light source. The background spectrum was measured after the pretreatment under a He gas flow at the 373 K. X-ray photoelectron spectroscopy (XPS) measurement was conducted on an ESCA-3400 spectrometer (Shimadzu, Japan). Sample was mounted on a silver sample holder by using a conductive carbon tape, and analyzed using Mg Kα radiation in a vacuum chamber in 0.1 eV steps. The position of the carbon peak (284.6 eV) for C1s was used to calibrate the binding energy for all the samples. The surface atomic ratio was estimated from the band areas of XPS of Ba 3d, and Ti 2p, and the corresponding relative sensitivity factors [39]. Transmission electron microscopy (TEM) observation was carried out with JEOL-1400 TEM (JEOL, Japan).

3. Results and discussion

3.1. Effect of Ba loading

Fig. 1A represents the time course of NO_x storage over Ba/TiO_2 catalysts with various Ba loadings. Without a catalyst, NO_x concentration increased to 200 ppm immediately at the same time as NO/O_2 gas was introduced to the reactor. TiO_2 showed activity for NO_x storage under UV-light irradiation, and the dead time for the NO_x breakthrough was 530 s. Loading of Ba drastically extended the dead time for NO_x breakthrough for all the Ba loadings investigated as compared to TiO_2. Fig. 1B shows the dead time in Fig. 1A as a function of Ba loading. The dead time increased with increasing the Ba loading up to 500 μmol g^{-1}, and deceased over 500 μmol g^{-1}. The dead time in 500 μmol g^{-1} Ba/TiO_2 was 1020 s, which was longer than the period during the cold start condition (800 s) reported by ICCT [11]. After the reaction after 12 h, the rates of NO_x storage were saturated, and the total amounts of stored NO_x for 12 h of 500 μmol g^{-1} Ba/TiO_2 and TiO_2 were 560 and 389 μmol g^{-1}, respectively. The modification of TiO_2 with Ba oxides species improved both the dead time and the total adsorption amount of NO_x.

The XRD patterns of TiO_2 and as-synthesized Ba/TiO_2 with various Ba loading showed diffraction peaks of anatase TiO_2 (Fig. 2). Diffraction peaks of cubic $Ba(NO_3)_2$ appeared in the as-synthesized Ba/TiO_2 catalysts over 250 μmol g^{-1} of Ba loading, which indicates that the Ba species are loaded on TiO_2 as a nitrate form after the

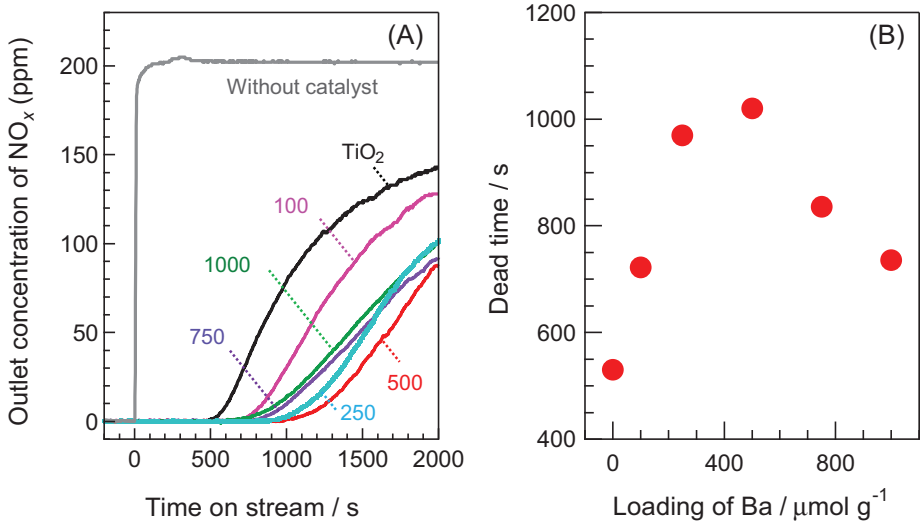

Fig. 1. (A) Time course of the photoassisted NO_x storage over Ba/TiO_2 catalysts. Pretreatment temperature: 773 K, NO: 200 ppm, O_2: 2%, He: balance. The numbers represent Ba loadings ($\mu mol\,g^{-1}$). (B) Effect of Ba loading on the dead time for the NO_x breakthrough.

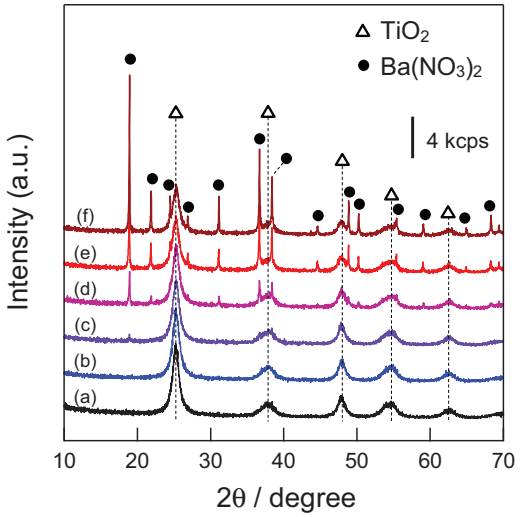

Fig. 2. XRD patterns of the as-synthesized Ba/TiO_2 catalysts with various Ba loading. (a) 0, (b) 100, (c) 250, (d) 500, (e) 750, and (f) 1000 $\mu mol\,g^{-1}$.

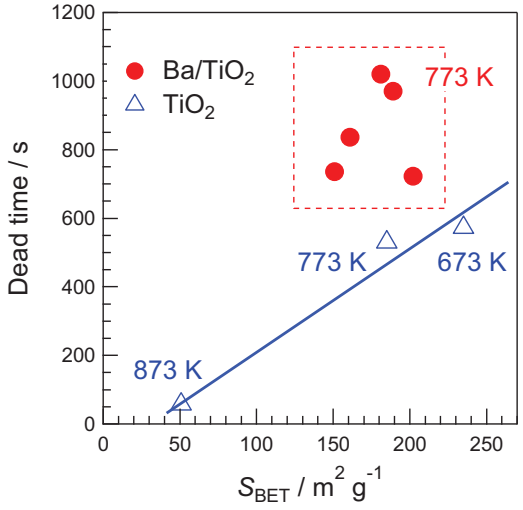

Fig. 3. Correlation between S_{BET} and the dead time for the NO_x breakthrough. Pretreatment temperatures were shown next to the symbols.

impregnation. Table 1 represents the crystalline size of TiO_2 and S_{BET} of the catalysts with various Ba loading. In the as-synthesized catalysts, S_{BET} decreased with increasing the Ba loading although the crystalline size of TiO_2 did not change after the Ba loading. The decrease of the surface area is possibly due to a plugging of pores derived from gaps of TiO_2 particles [40]. Without Ba loading (bare TiO_2), the pretreatment at 773 K and the following reaction drastically decreased S_{BET} from 292 to 185 $m^2\,g^{-1}$ and increased the crystalline sizes of TiO_2 from 7.7 to 10.9 nm, which was due to sintering of TiO_2 particles after the pretreatment at 773 K. The crystalline sizes of TiO_2 (8.5–9.3 nm) in Ba/TiO_2 after the reaction were smaller than that of TiO_2 after the reaction (10.9 nm). Thus, the Ba loading clearly suppressed the sintering of TiO_2 particles. To investigate of the effect of S_{BET}, the dead time was plotted as a function of S_{BET} as shown in Fig. 3. The dead time increased with increasing S_{BET} in the case of TiO_2 after the pretreatment at 673, 773, and 873 K (blue triangles). In the several photocatalytic reactions [21,41], the activity strongly depends on the surface area of the photocatalyst especially when the adsorption step of substrates is relatively slow. In this reaction, the strong positive correlation between the dead time and S_{BET} was clearly observed, which suggests that the increase of S_{BET} would be effective to improve the activity. On the other hand, Ba/TiO_2 photocatalyst (red circles) showed the significantly higher activity than those of TiO_2 with similar S_{BET}. The activity improvement by the Ba loading cannot be explained by the surface area (i.e., sintering of TiO_2 particles). In addition, there was

Table 1
Crystalline size of TiO_2 and BET specific surface area before and after the pretreatment and reaction.

Ba loading	d[a] (nm)		S_{BET}[b] ($m^2\,g^{-1}$)	
($\mu mol\,g^{-1}$)	As-syn.[c]	AR[d]	As-syn.	AR
0	7.7	10.9	292	185
100	7.6	9.3	272	202
250	7.6	9.2	254	189
500	7.5	8.8	228	181
750	7.7	8.5	204	161
1000	7.7	8.5	181	151

[a] Crystalline size of TiO_2.
[b] Specific surface area estimated from the BET method.
[c] As-synthesized.
[d] After the pretreatment at 773 K and the following NO_x storage reaction.

no correlation between the dead time and S_{BET} in Ba/TiO_2 with various Ba loading, which suggests that the dead time is dependent on the amount and state of Ba species. The total amount of stored NO_x for 12 h of 500 μmol g^{-1} Ba/TiO_2 was 1.4 times higher than that of TiO_2 although S_{BET} was almost the same as shown in Table 1. The results suggested that the Ba oxide species generated after the pretreatment at 773 K functioned as an effective NO_x storage material.

3.2. Correlation of the activity and TPD peak areas

TPD experiments were carried out using the as-synthesized Ba/TiO_2 catalysts to identify the active Ba precursors (Fig. 4A). Three desorption peaks were observed around 710, 800, and 850 K (referred to as peaks 1–3, respectively). The peak 1 was assigned to the decomposition of $Ba(NO_3)_2$ in contact with a TiO_2 surface, and the peaks 2 and 3 were due to the decomposition of bulk $Ba(NO_3)_2$ [29]. Two desorption peaks were observed in the TPD experiment using a $Ba(NO_3)_2$ reference powder at 840 and 910 K, and the desorption temperatures were higher than those of Ba/TiO_2. The low desorption temperatures in the Ba-modified catalysts were due to the interaction between TiO_2 and Ba species [38]. The peaks 2 and 3 were possibly due to the decomposition of the surface and inner part of bulk $Ba(NO_3)_2$ [29]. The areas of peaks 1–3, which were estimated from a peak fitting using three Gaussians were plotted against the Ba loading (Fig. 4B). The area of peak 1 increased with the Ba loading up to 500 μmol g^{-1}, and was saturated over 500 μmol g^{-1}. On the other hands, the areas of peaks 2 and 3 showed the same tendency; the areas of two peaks were low below 250 μmol g^{-1}, and the further increase of the Ba loading rapidly increased the areas of the two peaks. The same tendency supports the above assignment that peaks 2 and 3 were derived from the bulk $Ba(NO_3)_2$. As shown above, there are at least two $Ba(NO_3)_2$ species in the as-synthesized Ba/TiO_2; one is the surface $Ba(NO_3)_2$ in contact with a TiO_2 surface, and the other one is the bulk $Ba(NO_3)_2$ without a contact with a TiO_2 surface.

The effect of the Ba loading on the activity was explained by the amount of two $Ba(NO_3)_2$ species estimated from the TPD spectra. The dead time in Fig. 1 increased with increasing the area of peak 1 derived from the surface $Ba(NO_3)_2$. The correspondence between activity and the amount of surface $Ba(NO_3)_2$ indicated that the surface $Ba(NO_3)_2$ on a TiO_2 is a precursor of active Ba oxide species for the NO_x storage. On the other hand, over 500 μmol g^{-1}, the activity decreased in spite of the fact that the amount of the surface $Ba(NO_3)_2$ (i.e., area of peak 1) did not change. The bulk $Ba(NO_3)_2$, which was inactive for the reaction [29] was generated, and the amount increased with the Ba loading. The increase of the Ba loading from 500 to 1000 μmol g^{-1} decreased the TiO_2 content in the catalyst by 13 wt% because the 500 and 1000 μmol g^{-1} corresponded to 13 and 26 wt%, respectively. The decrease of TiO_2 should decrease the activity because TiO_2 works as an oxidation site in the reaction. Thus, amounts of the surface $Ba(NO_3)_2$ and the inactive bulk $Ba(NO_3)_2$ affected the activity, which resulted in the non-correlation between S_{BET} and the activity in Ba/TiO_2 in Fig. 3.

3.3. DRIFT investigation

DRIFT spectra were recorded at various exposure times of NO/O_2 gas in the dark. In the case of TiO_2 (Fig. 5A), the peaks at 1622, 1480, 1322, and 1194 cm^{-1} increased with the exposure time of NO/O_2 gas. The peaks at 1480, 1322, and 1194 cm^{-1} were assignable to NO_2^- species, and the peak at 1622 cm^{-1} to NO_3^- species [42]. The co-adsorption of NO and O_2 produced NO_2^- and NO_3^- species via adsorption and oxidation, which was in line with previous reports using several transition metals including TiO_2 [42–45]. After the irradiation, the peak intensity at 1194 cm^{-1} monotonically decreased with the irradiation time, which indicates that the NO_2^- species are consumed under irradiation. On the other hand, the intensities of new peaks at 1603, 1582, 1496, 1302, and 1249 cm^{-1} increase and are saturated after 20 min of irradiation, which is due to the generation of NO_3^- species with bridging (1603, 1249 cm^{-1}), chelating (1582, 1302 cm^{-1}), and monodentate (1496 cm^{-1}) forms [21,42,43]. Thus, the NO_2^- species are an intermediate in NO_x storage, and are oxidized into the NO_3^- species under irradiation (Eqs. (1) and (2)).

$$NO \xrightarrow{O_2,dark} NO_2^-, NO_3^- \quad (1)$$

$$NO \xrightarrow{O_2,hv} NO_3^- \quad (2)$$

DRIFT spectra in 500 μmol g^{-1} Ba/TiO_2 were shown in Fig. 5B. In the dark, peaks at 1620, 1477, 1379, and 1210 appeared after 30 min of an NO/O_2 gas flow, and attribute to NO_2^- and NO_3^- species adsorbed on Ti sites because the peaks were observed in the case of TiO_2. Other peaks were also observed at 1379 cm^{-1} and around 1200 cm^{-1} (shoulder peaks) in Ba/TiO_2, which is possibly due to the NO_2^- species [42]. Although a small difference was observed in the DRIFT spectra between TiO_2 and Ba/TiO_2 in the dark, the difference was not a direct evidence of the improvement of the activity by Ba loading under irradiation because the activity of NO_x storage was quite low (no dead time) in the dark over Ba/TiO_2 [29]. The DRIFT spectra of Ba/TiO_2 after irradiation in NO/O_2 gas were similar to that in the case of TiO_2; adsorption peaks at 1601, 1580, 1502, 1295, and 1254 cm^{-1} increase with increasing the irradiation time for 3 h. The previous reports using BaO/Al_2O_3 catalyst showed that NO_2 adsorbed on a BaO surface as ionic and bidentate NO_3^- species and the adsorbed NO_3^- shows the IR peaks at 1550 cm^{-1} (bidentate), and 1320 and 1410 cm^{-1} (ionic) [34,45]. In our DRIFT investigations, the bands were not observed under irradiation. The results clearly indicates that the bulk BaO is not generated on a TiO_2 surface after the pretreatment. Absence of bulk BaO species suggests that Ba species are strongly interacted with TiO_2 as reported previously [38].

3.4. XRD pattern and TEM image

Fig. 6 shows the XRD patterns of TiO_2 and 500 μmol g^{-1} Ba/TiO_2. In all the catalysts, the diffraction peaks of anatase TiO_2 were observed. In as-synthesized Ba/TiO_2, the diffraction patterns of $Ba(NO_3)_2$ was observed, and the pretreatment at 773 K deceased the peak intensities. The decrease of the peak intensities is due to the decomposition of $Ba(NO_3)_2$ on a TiO_2 surface based on the TPD results. No other peak was observed after the pretreatment at 773 K, which suggests the Ba oxide species had an amorphous structure. After the NO_x storage, the peaks derived from $Ba(NO_3)_2$ did not change compared to Ba/TiO_2 after the pretreatment. From TEM images (Fig. 7), the particle size of TiO_2 in the as-synthesized Ba/TiO_2 was approximately 7–9 nm, which accorded to the crystalline size estimated from XRD (Table 1). The particle size hardly changed after the pretreatment at 773 K, and the following reaction.

3.5. XPS measurement

Fig. 8A shows Ba $3d_{5/2}$ XPS of the Ba-modified catalysts. The peak positon of Ba $3d_{5/2}$ XPS of the as-synthesized Ba/TiO_2 was 779.9 eV. The peak positions in Ba/TiO_2 after the pretreatment and the following reaction were 780.2 and 780.1 eV, respectively, and peak shift was hardly observed. The positions in the Ba-modified catalysts were different from that in the $BaTiO_3$ reference sample (778.8 eV). In all the Ba-modified catalysts, the peak positions of Ti $2p_{3/2}$ were 458.4–458.5 eV (Fig. 8B), which were equal to that in TiO_2 (458.4 eV). In the case of $BaTiO_3$, the peak position was 458.1 eV and was higher by 0.3–0.4 eV compared to the Ba-modified

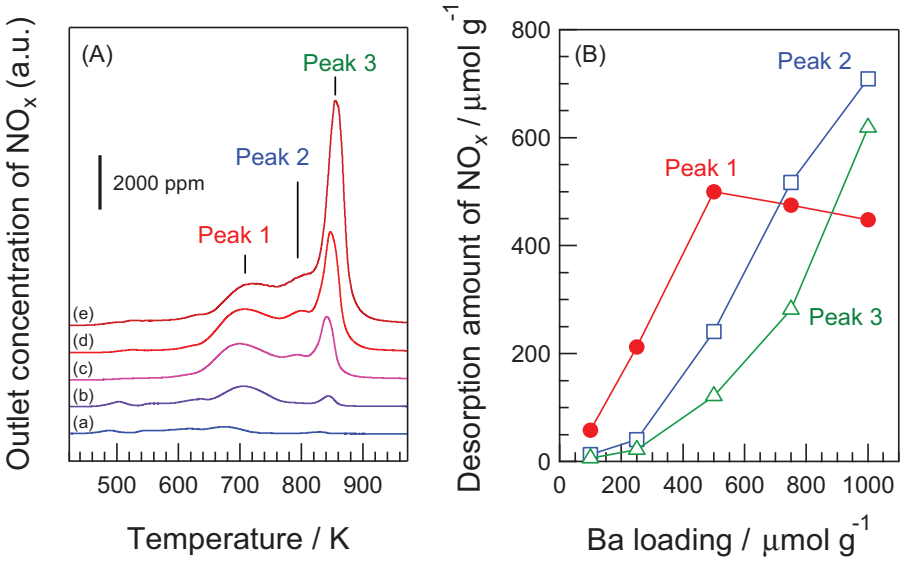

Fig. 4. (A) TPD profiles of as-synthesized Ba/TiO_2 catalyst with various Ba loadings of (a) 100, (b) 250, (c) 500, (d) 750, and (e) 1000 μmol g^{-1}. (B) Desorption amounts of NO_x estimated from the peaks 1–3 as a function of Ba loading.

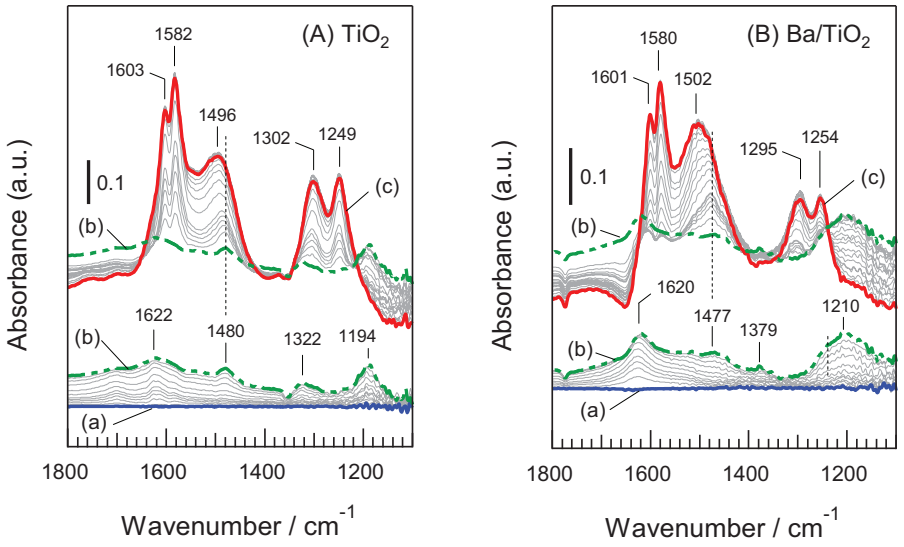

Fig. 5. DRIFT spectra of (A) TiO_2 and (B) 500 μmol g^{-1} Ba/TiO_2. After the pretreatment at 773 K: (a), after addition of NO/O_2 gas for 30 min in the dark: (b), after irradiation for 3 h in NO/O_2 gas: (c).

catalysts. The results indicate that the $BaTiO_3$ phase do not generated both after the pretreatment and the following reaction. The Ba/Ti surface atomic ratio was calculated from XPS. The pretreatment drastically increased the Ba/Ti ratio from 0.03 to 0.19, and decreased to 0.12 after the reaction. The increase in the Ba/Ti ratio clearly evidenced the structural change of Ba oxide species after the pretreatment, and can be explained by a two-dimensional layer structure of Ba oxide species. The two-dimensional structure of Ba species accorded with a model proposed by Emmez et al. using a substrate [46], and suggested the above-mentioned strong interaction between Ba oxide species and TiO_2.

3.6. Active Ba species in photoassisted NO_x storage

Surface model of the active Ba species for photoassisted NO_x storage is shown in Scheme 1. In as-synthesized catalysts, $Ba(NO_3)_2$ precursors are loaded on a TiO_2 surface. The O_2 pretreatment at 773 K decomposes the surface $Ba(NO_3)_2$ precursors to the active Ba species with an amorphous and two-dimensional layer structure with releasing NO_x. The DRIFT investigation revealed that the NO_3^- species were selectively adsorbed on Ti atoms after NO_x storage over Ba/TiO_2, which indicates that the generated NO_3^- species did not directly adsorb onto Ba atoms. In our previous reports,

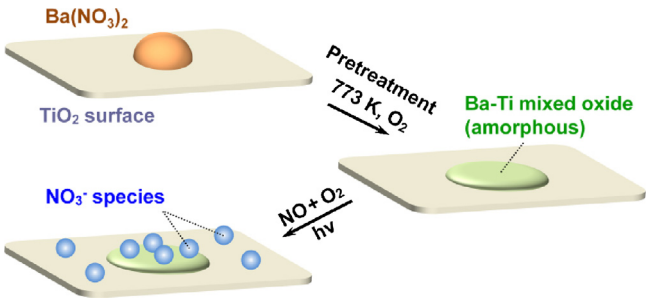

Scheme 1. Surface model of active Ba species for photoassisted NO_x storage.

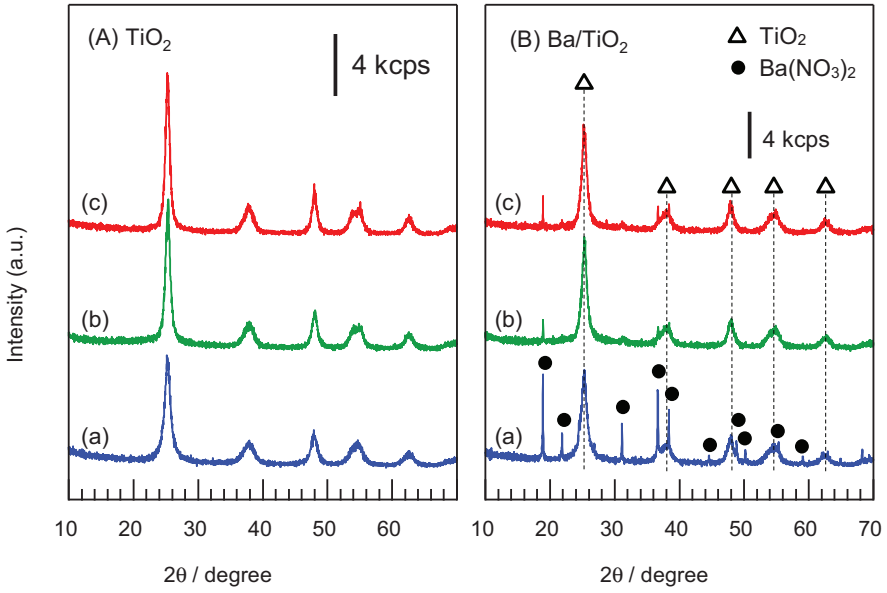

Fig. 6. XRD patterns of (A) TiO_2 and (B) 500 μmol g^{-1} Ba/TiO_2. (a): as-synthesized, (b): after the pretreatment at 773 K, (c): after the reaction.

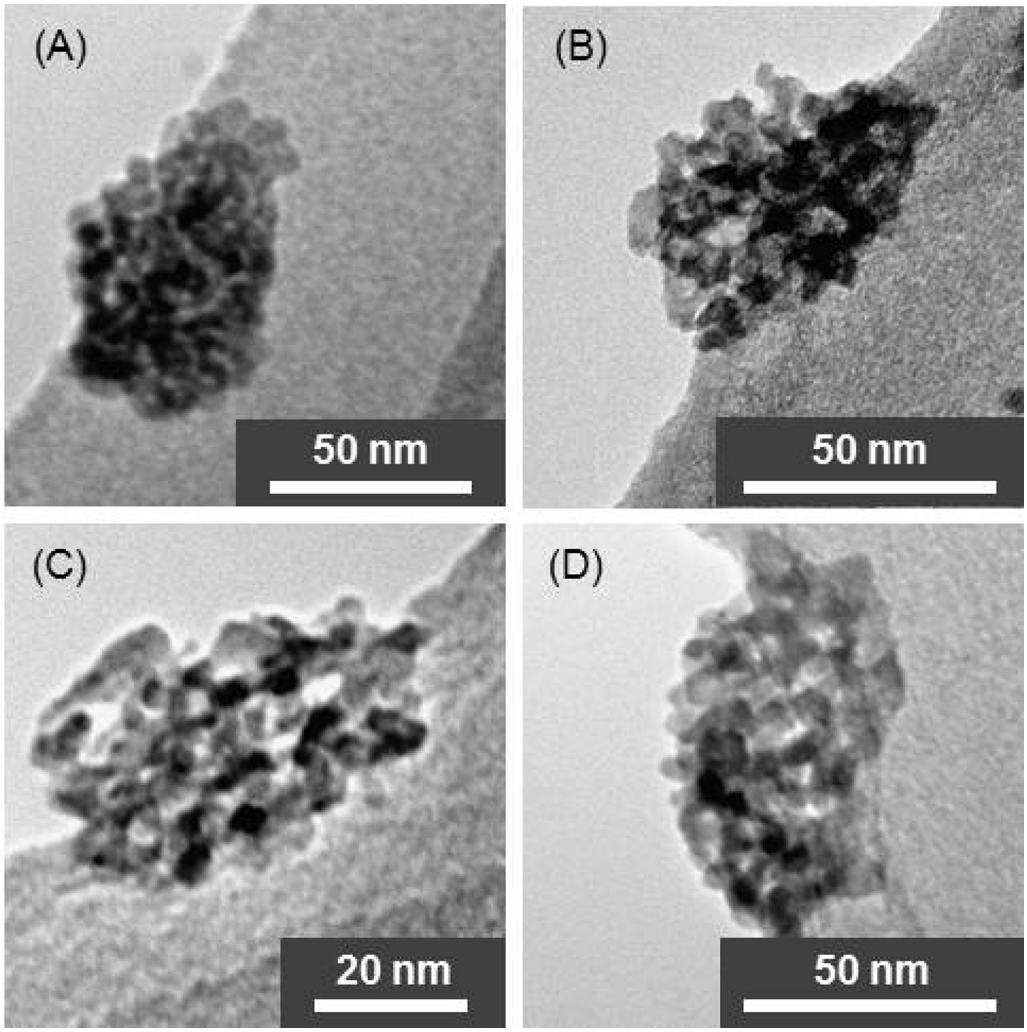

Fig. 7. TEM images of (A) TiO_2, (B) as-synthesized Ba/TiO_2, (C) Ba/TiO_2 after the pretreatment, and (D) Ba/TiO_2 after the reaction. Ba loading: 500 μmol g^{-1}.

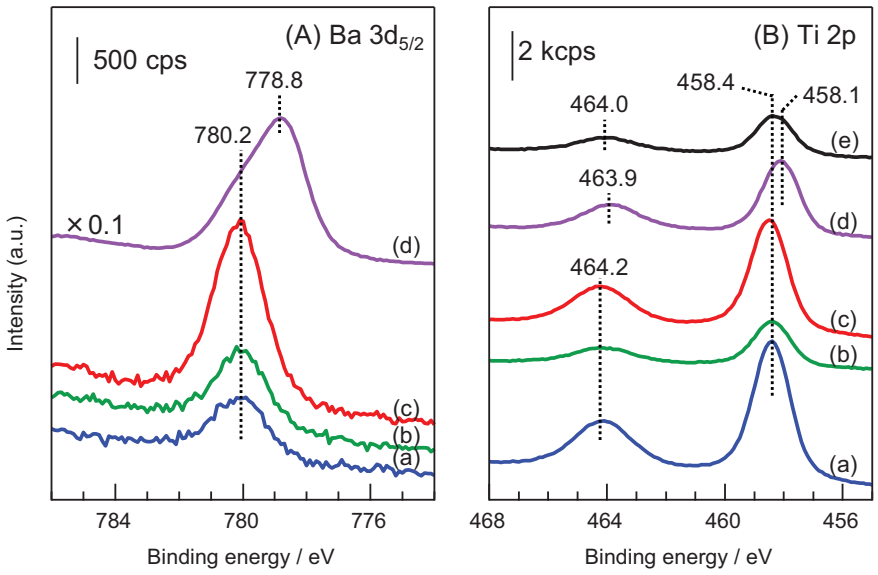

Fig. 8. XPS of (A) Ba $3d_{5/2}$ and (B) Ti 2p, (a): as-synthesized, (b): after the pretreatment at 773 K, (c): after the reaction, (d): $BaTiO_3$, (e): TiO_2.

XRD pattern showed the generation of $BaTiO_3$ phase after the O_2 pretreatment at 873 K [29]. Although the $BaTiO_3$ phase was not observed after the pretreatment at 773 K from the XRD pattern in this report, TPR experiments clearly showed the decomposition of a part of $Ba(NO_3)_2$ species after the pretreatment. Thus, the absence of bulk BaO species on a TiO_2 surface is possibly due to the generation of Ba–Ti mixed oxides on a TiO_2 surface with an amorphous structure. The generation of Ba–Ti mixed oxides coincide with the previous report by Emmez et al. [46]. They proposed the generation of perovskite-type Ba–Ti surface species (e.g., $BaTiO_3$, and Ba_2TiO_4) with an amorphous structure after Ba deposition over TiO_2 films on a Pt(1 1 1) single crystal and following oxidation by O_2 at 573–973 K using XPS and low energy electron diffraction (LEED). The selective adsorption of NO_3^- onto Ti atoms observed in our DRIFT experiment using Ba/TiO_2 suggests that the NO_3^- species were adsorbed on Ti sites on the Ba–Ti mixed oxides. Besides, the adsorption of NO_x on perovskite compounds including $BaTiO_3$ was investigated previously, and these perovskites showed a high NO_x storage capacity in spite of the low S_{BET}, (i.e., surface density of NO_x^- species was high on $BaTiO_3$) [47]. In our experiments, 500 μmol g^{-1} Ba/TiO_2 showed 1.4 times higher NO_x storage capacity than the non-modified TiO_2 despite the similar S_{BET} values (Table 1). Thus, the amorphous Ba–Ti mixed oxides stored NO_3^- more densely than the TiO_2 surface. We concluded that the Ba–Ti mixed oxides on a TiO_2 surface function as an effective NO_x storage material and the generation leads to the high activity in photoassisted NO_x storage under UV-light irradiation.

4. Conclusions

We demonstrated the surface modification of Ba species is an effective method to improve the activity in photoassisted NO_x storage over TiO_2-based photocatalysts under UV-light irradiation. The Ba loading affected the amounts of the surface and bulk $Ba(NO_3)_2$ species in the as-synthesized catalysts, and the amounts predominated the activity. We proposed that the surface $Ba(NO_3)_2$ was decomposed after the O_2 pretreatment at 773 K into the active Ba–Ti mixed oxides with an amorphous and two-dimensional layer structure. The surface Ba–Ti mixed oxides functioned as an effective NO_x storage material, which leads to the high activity of the Ba-modified TiO_2 photocatalysts.

Acknowledgments

This study was partially supported by the Program for Element Strategy Initiative for Catalysts & Batteries (ESICB), commissioned by the Ministry of Education, Culture, Sports, Science and Technology (MEXT) of Japan, and the Precursory Research for Embryonic Science and Technology (PRESTO), supported by the Japan Science and Technology Agency (JST). Akira Yamamoto thanks the JSPS Research Fellowships for Young Scientists.

References

[1] S. Roy, A. Baiker, Chem. Rev. 109 (2009) 4054–4091.
[2] G. Centi, G.E. Arena, S. Perathoner, J. Catal. 216 (2003) 443–454.
[3] J. Kašpar, P. Fornasiero, N. Hickey, Catal. Today 77 (2003) 419–449.
[4] G. Liu, P.-X. Gao, Catal. Sci. Technol. 1 (2011) 552–568.
[5] H. Takahashi, T. Shinjoh, T. Iijima, K. Suzuki, K. Yamazaki, H. Yokota, N. Suzuki, T. Matsumoto, T. Tanizawa, S.-S. Tateishi, K. Kasahara, Catal. Today 27 (1996) 63–69.
[6] G. Busca, L. Lietti, G. Ramis, F. Berti, Appl. Catal. B 18 (1998) 1–36.
[7] V.I. Pârvulescu, P. Grange, B. Delmon, Catal. Today 46 (1998) 233–316.
[8] P. Forzatti, Appl. Catal. A 222 (2001) 221–236.
[9] J. Li, H. Chang, L. Ma, J. Hao, R.T. Yang, Catal. Today 175 (2011) 147–156.
[10] T. Johnson, Platinum Met. Rev. 52 (2008) 23–37.
[11] L. Dana, K. Fanta, Urban off-cycle NO_x emissions from Euro IV/V trucks and buses, <http://www.theicct.org/urban-cycle-nox-emissions-euro-ivv-trucks-and-buses/> (2012).
[12] Y. Matsumoto, H. Ikeda, M. Suzuki, N. Ogai, Appl. Catal. B 25 (2000) 115–124.
[13] W.S. Epling, L.E. Campbell, A. Yezerets, N.W. Currier, J.E. Parks, Catal. Rev.: Sci. Eng. 46 (2004) 163–245.
[14] N. Takahashi, K. Yamazaki, H. Sobukawa, H. Shinjoh, Appl. Catal. B 70 (2007) 198–204.
[15] Y. Ohko, Y. Nakamura, N. Negishi, S. Matsuzawa, K. Takeuchi, J. Photochem. Photobiol. A 205 (2009) 28–33.
[16] S. Yin, H. Yamaki, M. Komatsu, Q. Zhang, J. Wang, Q. Tang, F. Saito, T. Sato, Solid State Sci. 7 (2005) 1479–1485.
[17] Y. Ishibai, J. Sato, S. Akita, T. Nishikawa, S. Miyagishi, J. Photochem. Photobiol. A 188 (2007) 106–111.
[18] K. Hashimoto, K. Sumida, S. Kitano, K. Yamamoto, N. Kondo, Y. Kera, H. Kominami, Catal. Today 144 (2009) 37–41.
[19] B.N. Shelimov, N.N. Tolkachev, O.P. Tkachenko, G.N. Baeva, K.V. Klementiev, A.Y. Stakheev, V.B. Kazansky, J. Photochem. Photobiol. A 195 (2008) 81–88.
[20] A.M. Soylu, M. Polat, D.A. Erdogan, Z. Say, C. Yıldırım, Ö. Birer, E. Ozensoy, Appl. Surf. Sci. 318 (2014) 142–149.
[21] K. Hashimoto, K. Wasada, N. Toukai, H. Kominami, Y. Kera, J. Photochem. Photobiol. A 136 (2000) 103–109.
[22] J. Lasek, Y.-H. Yu, J.C.S. Wu, J. Photochem. Photobiol. C 14 (2013) 29–52.
[23] R. Dillert, A. Engel, J. Große, P. Lindner, D.W. Bahnemann, Phys. Chem. Chem. Phys. 15 (2013) 20876–20886.
[24] A. Folli, S.B. Campbell, J.A. Anderson, D.E. Macphee, J. Photochem. Photobiol. A 220 (2011) 85–93.

[25] Q. Wu, R. van de Krol, J. Am. Chem. Soc. 134 (2012) 9369–9375.
[26] J. Zhang, T. Ayusawa, M. Minagawa, K. Kinugawa, H. Yamashita, M. Matsuoka, M. Anpo, J. Catal. 198 (2001) 1–8.
[27] J.C.S. Wu, Y.-T. Cheng, J. Catal. 237 (2006) 393–404.
[28] J.S. Dalton, P.A. Janes, N.G. Jones, J.A. Nicholson, K.R. Hallam, G.C. Allen, Environ. Pollut. 120 (2002) 415–422.
[29] A. Yamamoto, Y. Mizuno, K. Teramura, S. Hosokawa, T. Tanaka, ACS Catal. 5 (2015) 2939–2943.
[30] S. Hodjati, P. Bernhardt, C. Petit, V. Pitchon, A. Kiennemann, Appl. Catal. B 19 (1998) 209–219.
[31] S. Hodjati, P. Bernhardt, C. Petit, V. Pitchon, A. Kiennemann, Appl. Catal. B 19 (1998) 221–232.
[32] D.H. Kim, J.H. Kwak, J. Szanyi, S.D. Burton, C.H.F. Peden, Appl. Catal. B 72 (2007) 233–239.
[33] D. Uy, A. O'Neill, J. Li, W.H. Watkins, Catal. Lett. 95 (2004) 191–201.
[34] S.M. Andonova, G.K.S. Şentürk, E. Ozensoy, J. Phys. Chem. C 114 (2010) 17003–17016.
[35] T. Tanaka, K. Amano, K. Dohmae, N. Takahashi, H. Shinjoh, Appl. Catal. A 455 (2013) 16–24.
[36] H. Imagawa, N. Takahashi, T. Tanaka, S.I. Matsunaga, H. Shinjoh, Appl. Catal. B 92 (2009) 23–29.
[37] I.S. Pieta, W.S. Epling, M. García-Diéguez, J.Y. Luo, M.A. Larrubia, M.C. Herrera, L.J. Alemany, Catal. Today 175 (2011) 55–64.
[38] S.M. Andonova, G.S. Şentürk, E. Kayhan, E. Ozensoy, J. Phys. Chem. C 113 (2009) 11014–11026.
[39] J.H. Scofield, J. Electron. Spectrosc. Relat. Phenom. 8 (1976) 129–137.
[40] A. Yamamoto, K. Teramura, S. Hosokawa, T. Tanaka, Sci. Technol. Adv. Mater. 16 (2015) 24901.
[41] S. Yamazoe, T. Okumura, T. Tanaka, Catal. Today 120 (2007) 220–225.
[42] K.I. Hadjiivanov, Catal. Rev.: Sci. Eng. 42 (2000) 71–144.
[43] G. Ramis, G. Busca, V. Lorenzelli, P. Forzatti, Appl. Catal. 64 (1990) 243–257.
[44] I. Nova, L. Castoldi, L. Lietti, E. Tronconi, P. Forzatti, F. Prinetto, G. Ghiotti, J. Catal. 222 (2004) 377–388.
[45] F. Prinetto, G. Ghiotti, I. Nova, L. Castoldi, L. Lietti, E. Tronconi, P. Forzatti, Phys. Chem. Chem. Phys. 5 (2003) 4428–4434.
[46] E. Emmez, E.I. Vovk, V.I. Bukhtiyarov, E. Ozensoy, J. Phys. Chem. C 115 (2011) 22438–22443.
[47] S. Hodjati, K. Vaezzadeh, C. Petit, V. Pitchon, A. Kiennemann, Appl. Catal. B 26 (2000) 5–16.